Regular Article

PHYSICAL CHEMISTRY RESEARCH
Published by the
Iranian Chemical Society
www.physchemres.org
info@physchemres.org

***Phys. Chem. Res.**, Vol. 7, No. 2, 435-447, June 2019*
DOI: 10.22036/pcr.2019.172026.1594

Molecular Interactions of MeOH and EtOH with Black Phosphorus Monolayer: A Periodic Density Functional Study

M. Ghambarian[a], M. Ghashghaee[b,*], Z. Azizi[c] and M. Balar[b,d]

[a]*Gas Conversion Department, Faculty of Petrochemicals, Iran Polymer and Petrochemical Institute, P. O. Box: 14975-112, Tehran, Iran*
[b]*Faculty of Petrochemicals, Iran Polymer and Petrochemical Institute, P. O. Box: 14975-112, Tehran, Iran*
[c]*Department of Chemistry, Karaj Branch, Islamic Azad University, P. O. Box: 31485-313, Karaj, Iran*
[d]*Young Researchers and Elite Club, Karaj Branch, Islamic Azad University, Karaj, Iran*
(Received 13 February 2019, Accepted 13 May 2019)

The adsorption properties of black phosphorus monolayer (BPML) nanostructure toward methanol and ethanol were investigated using periodic density functional theory calculations. Despite the subtle in-plane distortions, the integrity of the BPML nanostructure was preserved. All complexes revealed interactions of pure electrostatic nature as evinced by the LOL and QTAIM data. The band gap was slightly enlarged, and both valence and conduction bands moved upward upon the detection of both alcohols. These observations implied that the perfect surface of the semiconductor could be considered as a work function sensor for the alcohol molecules. The adsorption energy ranged from -0.13 to -0.36 eV, with relatively stronger physisorption for ethanol.

Keywords: Black phosphorus, Adsorption, Methanol, Ethanol, DFT

INTRODUCTION

The isolation of few-layer flakes of black phosphorus using mechanical exfoliation unleashed a flurry of activities to investigate their physical and chemical properties in the realm of two-dimensional (2D) materials [1]. Compared to the other two well-known morphologies of phosphorus (white and red phosphorus), black phosphorus is more chemically stable and more resistant to ignition by fire. It also shows remarkable in-plane anisotropies and appreciable electron and heat conductance over white and red phosphorus [2-5].

In earlier studies, several authors have investigated the properties and applications of phosphorene nanostructures [3,6-7]. Kuo *et al*. [6] investigated the adsorption of NO, NO_2, NH_3, CO and CO_2 molecules on a phosphorene layer using density functional theory (DFT). The authors reported the superior molecular sensing of phosphorene compared to graphene which was attributed to the enhanced charge transfer between the molecules and phosphorene.

Methanol (MeOH) and ethanol (EtOH) are two of the most widely used alcohols with widespread applications in automotive fuels, food, biomedical and chemical industries including colors, dyes, drugs, perfumes, *etc*. Both alcohol molecules can result in health problems such as headache, drowsiness, irritation of eyes and difficulty in breathing. Contrary to EtOH, MeOH is highly toxic with the danger of acidosis, dermatitis and blindness. Poisoning by MeOH is more severe leading to nausea, abdominal pain, shortness of breath, blurred vision, and dizziness. However, due to the extensive use of EtOH as a beverage, it is viewed as a common cause of car accidents, thus making the quantitative detection of EtOH vapor of both medically and socially importance [8-10]. Therefore, many researchers have investigated the adsorption of MeOH and EtOH on different materials from the theoretical point of view [8,11-20]. Esrafili and Nurazar [12] studied the dissociative adsorption of MeOH on the (6,0) zigzag boron nitride

*Corresponding author. E-mail: m.ghashghaee@ippi.ac.ir

nanotube structure. Lazar *et al.* [13] presented combined experimental/theoretical results for the adsorption of ethanol on pristine graphene. Recently, Mayorga-Martinez *et al.* [11] demonstrated the high sensitivity and selectivity of black phosphorus toward MeOH vapor. However, no computational studies have been implemented on the interactions of these alcohols on black phosphorus type structures.

In this paper, we report the structural and electronic properties of the adsorption complexes formed from the interactions of MeOH and EtOH with the surface of black phosphorus monolayer (BPML) nanostructure. For this purpose, the changes in the electronic properties, adsorption energies, and the band gap of the material upon alcohol adsorption are presented. To our knowledge, there is no computational report on the comparative adsorption of MeOH and EtOH on the nanoclusters of BPML. The obtained results will be useful in providing further insights into the properties of the rediscovered black phosphorus toward industrially and environmentally important molecules.

COMPUTATIONAL METHOD

The original crystal structure of phosphorene was taken from the established previous reports [21]. Two alcohol molecules (CH_3OH and C_2H_5OH) were adsorbed on the plausible sites of a pristine phosphorene unit cell by relaxing all atoms of the guest molecule and the nearby P atoms until the system was fully optimized; therefore, two different periodic systems containing 22 and 25 atoms were considered. A vacuum space of >20 Å along the *c*-axis was placed to avoid mirror interactions. The 20 *k*-points were included in the band structure calculation for the reference black phosphorus material. The adsorption energies of the alcohol molecules on the black phosphorus nanostructure were calculated by [22-24]:

$$\Delta E_{ads} = E_{BP\text{-}alcohol} - (E_{alcohol} + E_{BPML}) \quad (1)$$

where BP-alcohol is the adsorption complex with the related alcohol, BPML is the bare black phosphorous monolayer, and alcohol is either MeOH or EtOH vapor molecule.

The computations were performed using NWChem 6.5 [25] and Multiwfn 3.3.8 [26] . Burai 1.3 [27] was used for electronic property simulation. The main graphical outputs were generated by Mercury 3.6 [28-29]. The Perdew-Burke-Eernzerh (PBEPBE) functional [30-31] with the 6-31G* basis set [32-33] were applied to the optimizations. The energetic data were obtained using the hybrid functional Heyd-Scuseria-Ernzerhof (HSE06) [34-36] coupled with the 6-311G* basis set [37-38].

The analysis of the quantum theory of atoms in molecules (QTAIM) [39-43] was performed at the HSE06/6-311G* level of theory. The same functional and basis set were employed to calculate the energy levels of the valence and conduction bands and the associated band gap according to the frontier molecular orbital (FMO) theory [44].

1. RESULTS AND DISCUSSION

In theoretical studies [45-47], three highly symmetric sites, including T site (on top of a P atom), H site (a hollow site on top of a puckered hexagon), and B site (a bridge location at the midpoint of the P-P bond), are usually considered for the stabilization of adatoms on BPML. However, the adsorption site for a molecule is expected to be a combination of the mentioned positions. The optimized geometries of the BP-MeOH and BP-EtOH adsorption complexes are shown in Fig. 1. More detailed configurations (from both side and top views) are shown in Fig. S1. As shown in Fig. 1, only one adsorption structure could be identified for the stabilization of each alcohol on the surface of BPML nanostructure. For both alcohols, the adsorption complex retained orientations in which the hydroxyl group remained closer to the surface, preferably at an H site. On the other hand, the carbon atom of MeOH and the C-C bond in EtOH mostly preferred T and B sites, while standing in a farther distance of the BPML surface.

The main geometric parameters are listed in Tables 1 and 2 for the three optimized structures. Relatively similar structural features were found in the structures obtained from the periodic calculations for the two alcohol molecules (Fig. 1 and Table 2); the θ(POC) values ranged from 95.6°-158.8° in BP-MeOH and 95.2°-158.4° in BP-EtOH. Furthermore, the r(P-O) values ranged from 3.19-4.71 Å in

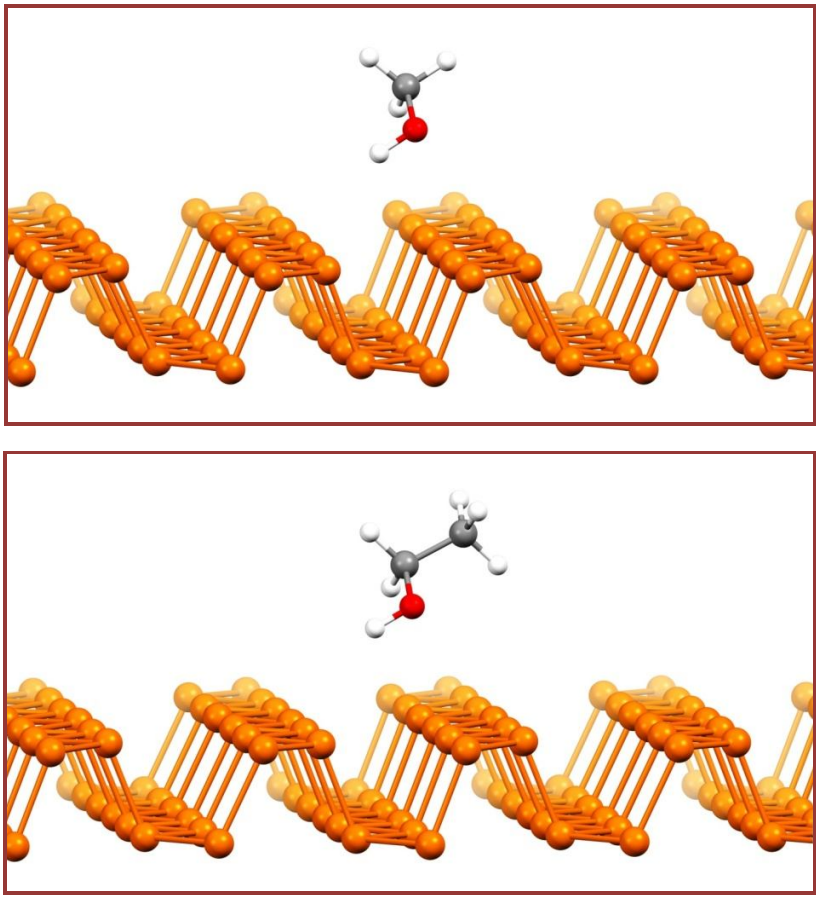

Fig. 1. Adsorption of methanol (top) and ethanol (bottom) on BPML, optimized at the PBEPBE/6-31G* level of theory. The orange balls represent phosphorus, the grey balls represent carbon, the red balls show oxygen, and the smaller white atoms are hydrogen.

Table 1. P-O and P-P Distances (Å) for Different Structures Optimized at the PBEPBE/6-31G* Level of Theory

Structure	P1-P5	P3-P7	P10-P6	P12-P8	P9-P13	P11-P15
BPML	2.30	2.30	2.30	2.30	2.30	2.30
BP-MeOH	2.30	2.30	2.30	2.31	2.30	2.30
	P1-O	P2-O	P3-O	P10-O	P11-O	P12-O
	3.19	3.25	4.71	-	-	-
BP-EtOH	2.31	2.30	2.30	2.30	2.30	2.30
	P1-O	P2-O	P3-O	P10-O	P11-O	P12-O
	-	-	3.83	3.19	3.19	3.22

Table 2. Selected Interbond Angles (in Degrees) for Different Structures Optimized at the PBEPBE/6-31G* Level of Theory

Structure	P1-O-C	P2-O-C	P3-O-C	P10-O-C	P11-O-C	P12-O-C
BPML	-	-	-	-	-	-
BP-MeOH	158.8	121.3	95.6	-	-	-
BP-EtOH	-	-	113.3	95.2	120.4	158.4

Table 3. QTAIM Analysis and Bond Order (BO) at the HSE06/6-311G* Level of Theory

Structure	BCP, RCP and CCP	ρ	λ_1	λ_2	λ_3	$\nabla^2\rho$	BO
BP-MeOH	P1-O	0.010	-0.006	-0.005	0.044	0.033	0.115
	P2-O	0.009	-0.004	-0.003	0.037	0.030	0.141
	P3-O	0.011	-0.008	-0.006	0.045	0.031	0.106
	P10-H	0.009	-0.007	-0.007	0.040	0.025	-
	O-C	0.248	-0.439	-0.434	0.430	-0.443	1.306
	O-P2-P1	0.009	-0.005	0.003	0.033	0.031	-
	O-P2-P3	0.009	-0.005	0.003	0.033	0.031	-
	O-H-P1-P10	0.005	-0.003	0.008	0.012	0.017	-
	O-H-P3-P10	0.005	-0.003	0.008	0.011	0.016	-
	P1-P2-P3-P10-O-H	0.005	0.004	0.005	0.006	0.015	-
BP-EtOH	P10-O	0.012	-0.008	-0.006	0.046	0.032	0.103
	P11-O	0.010	-0.005	-0.003	0.038	0.030	0.104
	P12-O	0.010	-0.006	-0.005	0.044	0.033	0.108
	P3-H	0.008	-0.006	-0.006	0.035	0.023	-
	O-C	0.245	-0.442	-0.420	0.413	-0.449	1.151
	C-C	0.247	-0.470	-0.451	0.348	-0.573	0.121
	O-P10-P11	0.009	-0.006	0.003	0.034	0.031	-
	O-P11-P12	0.009	-0.005	0.004	0.033	0.032	-
	O-H-P3-P10	0.005	-0.003	0.007	0.010	0.015	-
	O-H-P3-P12	0.005	-0.002	0.007	0.011	0.016	-
	P3-P10-P11-P12-O-H	0.004	0.004	0.004	0.006	0.014	-

BP-MeOH and 3.19-3.83 Å in BP-EtOH. As can be seen in Table 1, the adsorption of alcohol molecules led to distortions in the structure of BPML by the elongations as large as 0.01 Å in the P-P bonds in the armchair direction. At the same time, the integrity of the BPML plane was preserved favorably after the adsorption of both alcohol molecules. The band structure for the parent black phosphorus model (Fig. S2) was also in fair agreement with those reported previously [3,48-52].

The QTAIM analysis of the adsorption complexes deepens our understanding of the nature of surface interactions [22-23,53-57]. Table 3 contains the topological data for the bond critical points (BCPs). Four BCPs have been formed during the sensing of alcohols by BPML. As is evident, BCPs were observed for both P…O and P…H interactions for both alcohols; each alcohol displayed three BCPs for the P…O interactions and one BCP for the P…H interactions, which dealt with the H atom of the hydroxyl group. Hence, none of the hydrogen atoms of the alkyl group was involved in the stabilization of both alcohols. However, the bond order for the BCPs was slightly larger for BP-MeOH than BP-EtOH. In addition, both alcohol molecules have shown four ring critical points (RCPs) and one cage critical point (CCP). The localized orbital locator (LOL) maps can also delineate the nature of chemical bonding in different complexes [7,58]. These contour plots are normally analyzed in terms of (3,-3) attractors (Γ) to provide recognizable patterns of the interactions around bond critical points. All of the interactions in the present study were purely electrostatic as evinced by the LOL maps depicted in Fig. 2. This conclusion is further supported by the values of electron density, hessian eigenvalue, and Laplacian of the electron density distribution (Table 3).

A valuable property that is worth exploring is the band gap of the BPML structure and possible changes after the interactions with the guest molecules. Figure 3 shows the band gaps and the projected DOS profiles of the original BPML and the adsorption structures. The DOS plots demonstrated that the band gap of the initial BPML sensor (1.58 eV at HSE06/6-311G*), which is quite reasonable relative to the experimental values of 1.5-2.0 eV, was slightly expanded (by 0.02 and 0.03 eV in BP-MeOH and BP-EtOH, respectively). However, both the valence and conduction bands shifted toward higher levels after the adsorption of both alcohols (refer, *e.g.*, to the changes in E_v and E_c of respectively +0.22 and +0.19 eV in the case of BP-EtOH). This indicates that the work function is decreased and the BPML nanostructure is a good work function sensor with respect to ethanol and methanol assuming that the Fermi energy level is nearly at the middle of the band gap. However, it is also expected that an external field can also help with sensing of the analytes on a more conventional conductivity sensing basis. Figure 3 also shows that the electron densities of states in the valence bands of all adsorption nanostructures were determined by mainly the p_z orbitals of BPML while the s orbitals of BPML predominantly contributed to the conduction band of the adsorption complex. From the PDOS plots in Fig. 3, it can be observed that the 3d orbitals of phosphorus also contributed to the total density of states, particularly at the higher energy level regions of the conduction band. The new states created by the alcohol molecules were located far from the band gap, with more notable contributions into the conduction bands.

Table 4 contains the adsorption energies calculated at the HSE06/6-311G* level of theory. The values of ΔE_{ads} for BP-MeOH and BP-EtOH were equal to -0.13 and -0.36 eV, respectively. This observation indicates that both alcohols have been physisorbed on the surface of BPML. From a sensing point of view, this implies that the adsorbed molecules can be sensed and released quickly. Although ethanol exhibits slightly stronger adsorption than methanol, it is still in the physisorption mode. This observation indicates that methanol could be desorbed slightly more rapid than ethanol, thus enjoying a relatively better recovery from the surface of BPML.

CONCLUSIONS

This study investigates the adsorption properties of black phosphorus monolayer (BPML) nanostructure toward MeOH and EtOH molecules. Only one adsorption configuration on hollow and top sites was found to be plausible for the adsorption of each alcohol. Subtle in-plane expansions (as large as 0.01 Å in the armchair direction) occurred to the original framework of BPML nanostructure with the adsorption of both MeOH and EtOH; however, the

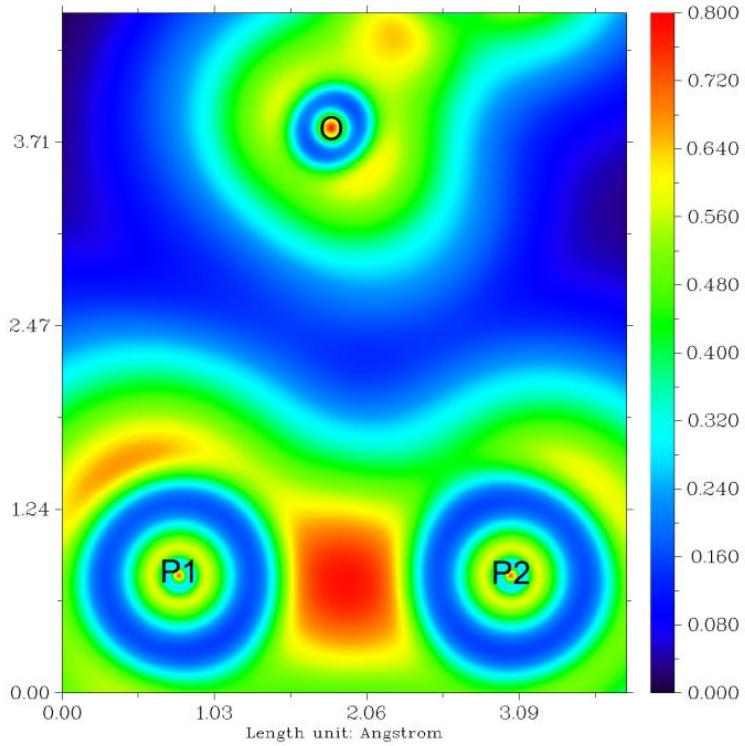

BP-MeOH

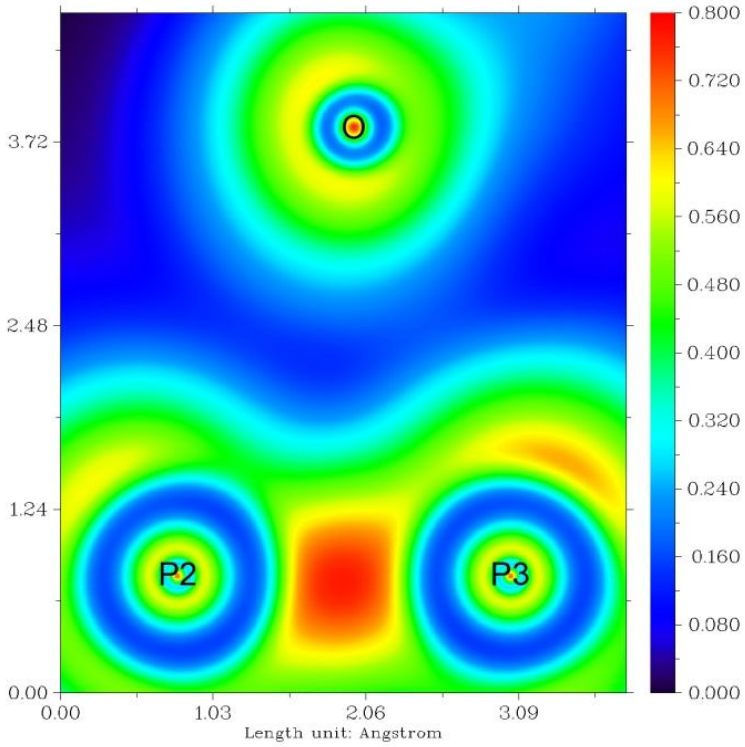

BP-MeOH

Fig. 2. LOL maps of the adsorption complexes at the vicinity of the alcohol molecules.

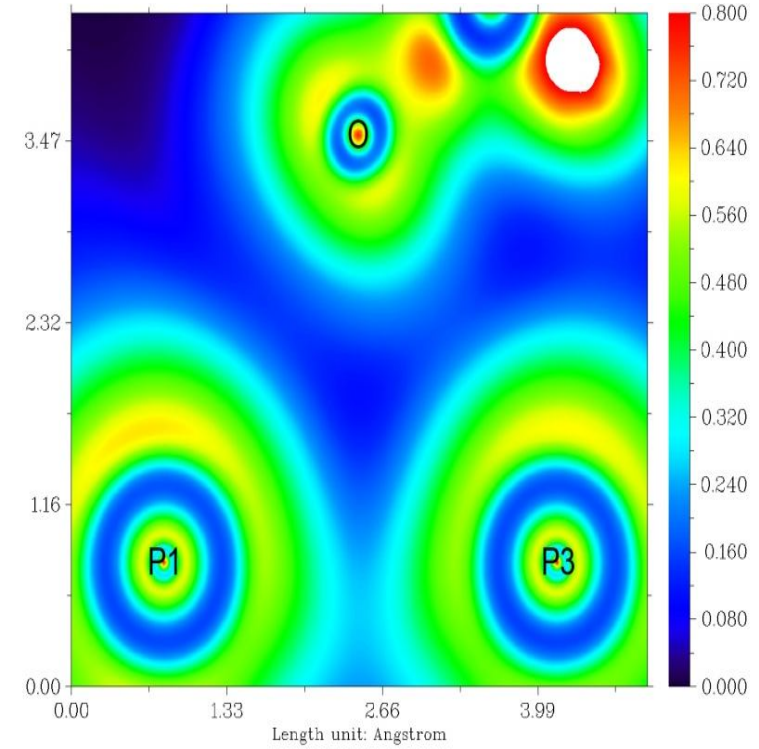

BP-MeOH

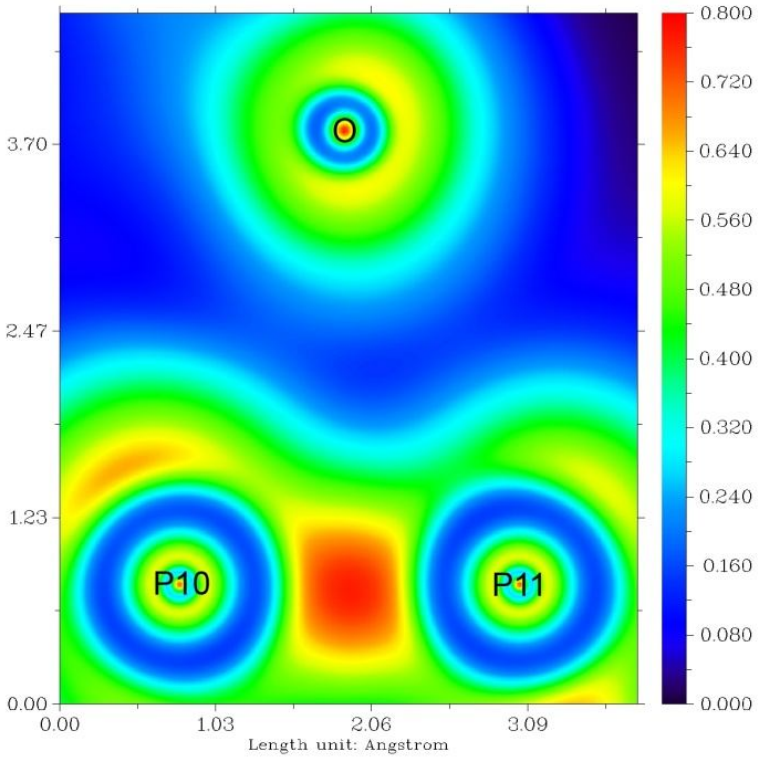

BP-EtOH

Fig. 2. Continued.

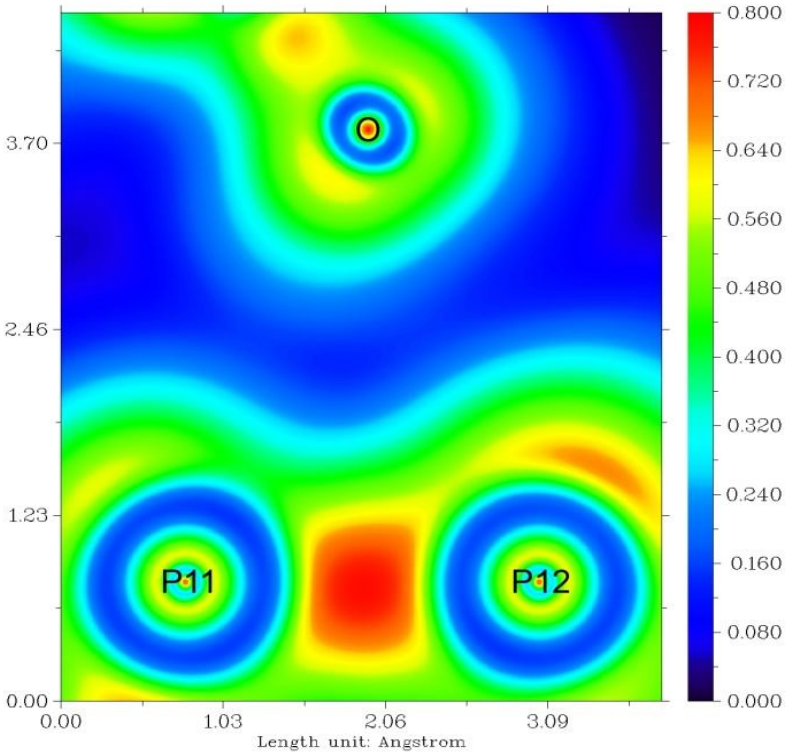

BP-EtOH

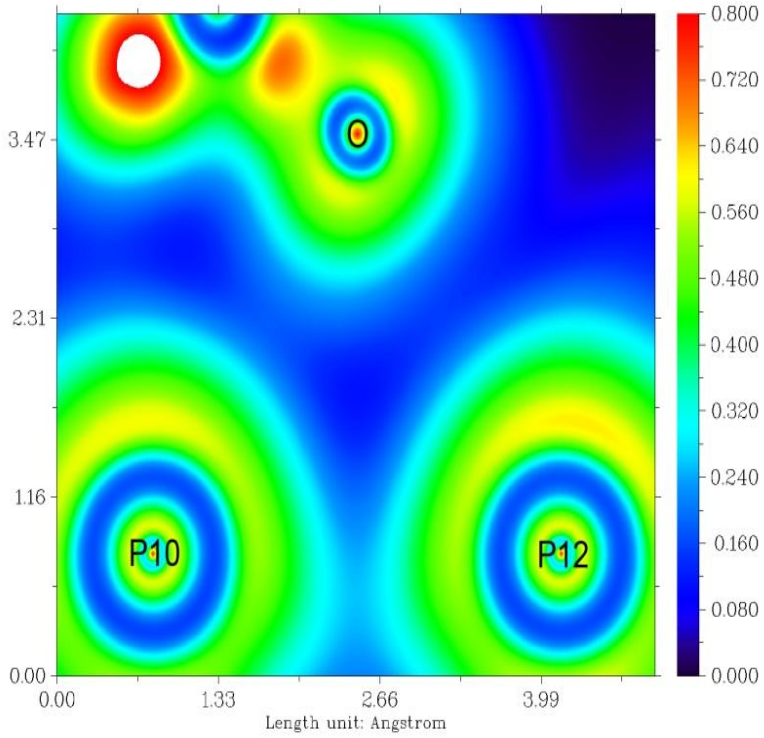

BP-EtOH

Fig. 2. Continued.

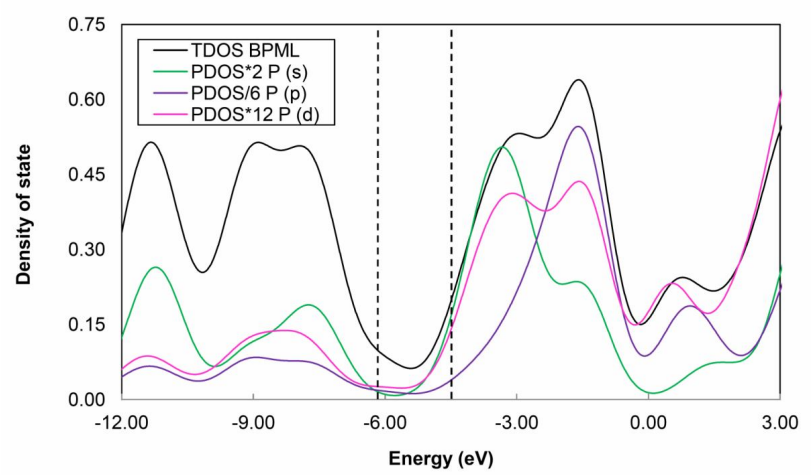

BPML

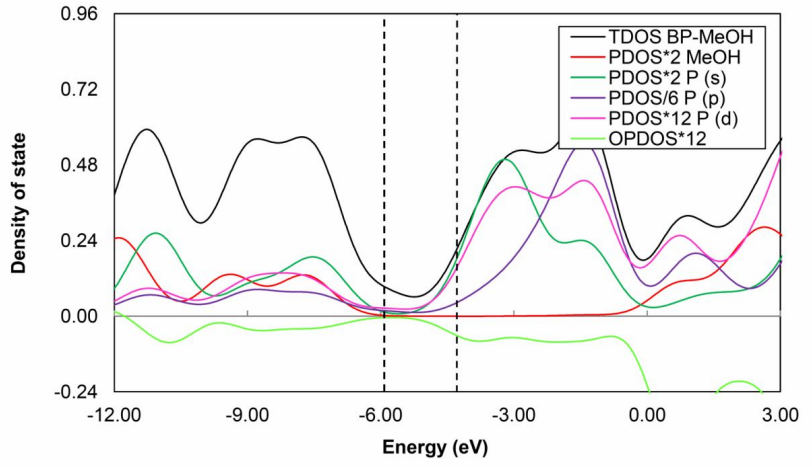

BP-MeOH

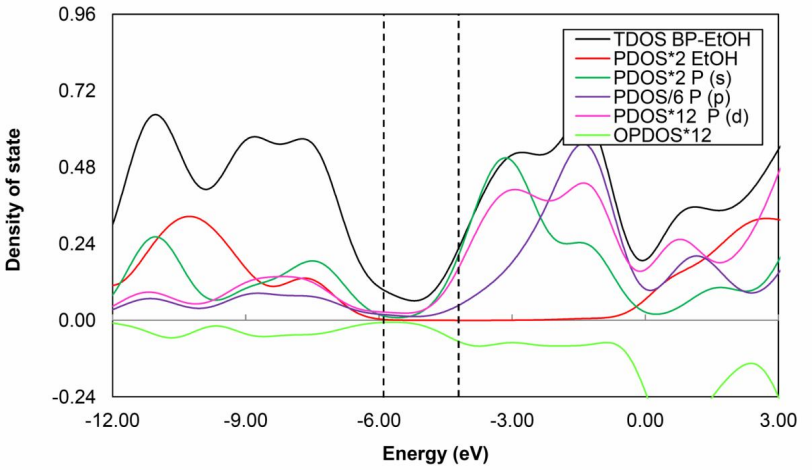

BP-EtOH

Fig. 3. TDOS and PDOS plots of the adsorption complexes.

Table 4. Adsorption Energy (kcal mol^{-1}) of the Alcohol Molecules at the HSE06/6-311G* Level of Theory

Adsorption complex	E_{ads}
BP-MeOH	-0.13
BP-EtOH	-0.36

integrity of the BPML nanostructure was preserved. All of the interactions were of pure electrostatic nature as confirmed by the LOL maps. The QTAIM analysis revealed the formation of three BCPs, four RCPs, and one CCP during the detection of each alcohol. The DOS plots demonstrated that the band gap of the initial BPML nanostructure was slightly expanded (by 0.02 and 0.03 eV for the adsorption of methanol and ethanol, respectively) in the absence of external electric manipulation. However, the valence and conduction bands shifted to higher energy levels for both alcohols. The adsorption energies of the alcohol molecules varied from -0.13 to -0.36 eV, while the stronger adsorption occured for the ethanol case.

REFERENCES

[1] Castellanos-Gomez, A.; Vicarelli, L.; Prada, E.; Island, J. O.; Narasimha-Acharya, K. L.; Blanter, S. I.; Groenendijk, D. J.; Buscema, M.; Steele, G. A.; Alvarez, J. V.; Zandbergen, H. W.; Palacios, J. J.; van der Zant, H. S. J., Isolation and characterization of few-layer black phosphorus. *2D Mater.* **2014**, *1*, 025001, DOI: 10.1088/2053-1583/1/2/025001.

[2] Jing, Y.; Zhang, X.; Zhou, Z., Phosphorene: what can we know from computations? *WIREs Comput. Mol. Sci.* **2016**, *6*, 5-19, DOI: 10.1002/wcms.1234.

[3] Sorkin, V.; Cai, Y.; Ong, Z.; Zhang, G.; Zhang, Y. W., Recent advances in the study of phosphorene and its nanostructures. *Crit. Rev. Solid State Mater. Sci.* **2017**, *42*, 1-82, DOI: 10.1080/10408436.2016.1182469.

[4] Lalitha, M.; Nataraj, Y.; Lakshmipathi, S., Calcium decorated and doped phosphorene for gas adsorption. *Appl. Surf. Sci.* **2016**, *377*, 311-323, DOI: 10.1016/j.apsusc.2016.03.119.

[5] Eswaraiah, V.; Zeng, Q.; Long, Y.; Liu, Z., Black phosphorus nanosheets: Synthesis, *Characterization and Applications. Small* **2016**, *12*, 3480-3502, DOI: 10.1002/smll.201600032.

[6] Kou, L.; Frauenheim, T.; Chen, C., Phosphorene as a superior gas sensor: Selective adsorption and distinct I-V response. *J. Phys. Chem. Lett.* **2014**, *5*, 2675-2681, DOI: 10.1021/jz501188k.

[7] Ghashghaee, M.; Ghambarian, M., Adsorption of toxic mercury, lead, cadmium, and arsenic ions on black phosphorous nanosheet: first-principles calculations. *Struct. Chem.* **2019**, *30*, 85-96, DOI: 10.1007/s11224-018-1173-6.

[8] Mirzaei, A.; Leonardi, S. G.; Neri, G., Detection of hazardous volatile organic compounds (VOCs) by metal oxide nanostructures-based gas sensors: A review. *Ceram. Int.* **2016**, *42*, 15119-15141, DOI: 10.1016/j.ceramint.2016.06.145.

[9] Patel, N. G.; Patel, P. D.; Vaishnav, V. S., Indium tin oxide (ITO) thin film gas sensor for detection of methanol at room temperature. *Sensor. Actuat. B-Chem.* **2003**, *96*, 180-189, DOI: 10.1016/S0925-4005(03)00524-0.

[10] Kadir, R. A.; Rani, R. A.; Zoolfakar, A. S.; Ou, J. Z.; Shafiei, M.; Wlodarski, W.; Kalantar-zadeh, K., Nb_2O_5 Schottky based ethanol vapour sensors: Effect of metallic catalysts. *Sensor. Actuat. B-Chem.* **2014**, *202*, 74-82, DOI: 10.1016/j.snb.2014.04.083.

[11] Mayorga-Martinez, C. C.; Sofer, Z.; Pumera, M., Layered black phosphorus as a selective vapor sensor. *Angew. Chem.* **2015**, *127*, 14525-14528, DOI: 10.1002/ange.201505015.

[12] Esrafili, M. D.; Nurazar, R., A DFT study on the possibility of using boron nitride nanotubes as a dehydrogenation catalyst for methanol. *Appl. Surf. Sci.* **2014**, *314*, 90-96, DOI: https://doi.org/10.1016/j.apsusc.2014.06.148.

[13] Lazar, P.; Karlický, F.; Jurečka, P.; Kocman, M.; Otyepková, E.; Šafářová, K.; Otyepka, M., Adsorption of small organic molecules on graphene. *J. Am. Chem. Soc.* **2013**, *135*, 6372-6377, DOI: 10.1021/ja403162r.

[14] Pankewitz, T.; Klopper, W., Interaction of the alcohol molecules methanol and ethanol with single-walled

carbon nanotubes - A computational study. *Chem. Phys. Lett.* **2010**, *498*, 345-348, DOI: 10.1016/j.cplett.2010.09.008.

[15] Tang, Z. -R., The adsorption of methanol at the defective site of single-walled carbon nanotube. *Physica B: Condens. Matter* **2010**, *405*, 770-773, DOI: 10.1016/j.physb.2009.09.103.

[16] Ellison, M. D.; Morris, S. T.; Sender, M. R.; Brigham, J.; Padgett, N. E., Infrared and computational studies of the adsorption of methanol and ethanol on single-walled carbon nanotubes. *J. Phys. Chem. C* **2007**, *111*, 18127-18134, DOI: 10.1021/jp0763432.

[17] Pengfei, C.; Neng, L.; Xingzhu, C.; Wee-Jun, O.; Xiujian, Z., The rising star of 2D black phosphorus beyond graphene: synthesis, properties and electronic applications. *2D Mater.* **2018**, *5*, 014002, DOI: 10.1088/2053-1583/aa8d37.

[18] Rad, A. S., Density functional theory study of the adsorption of MeOH and EtOH on the surface of Pt-decorated graphene. *Physica E: Low Dimens. Syst. Nanostruct.* **2016**, *83*, 135-140, DOI: 10.1016/j.physe.2016.04.030.

[19] Schröder, E., Methanol Adsorption on Graphene. *J. Nanomater.* **2013**, 2013, *6*, DOI: 10.1155/2013/871706.

[20] Shokuhi Rad, A.; Valipour, P., Interaction of methanol with some aniline and pyrrole derivatives: DFT calculations. *Synth. Met.* **2015**, *209*, 502-511, DOI: 10.1016/j.synthmet.2015.08.021.

[21] Lange, S.; Schmidt, P.; Nilges, T., Au_3SnP_7@Black phosphorus: An easy access to black phosphorus. *Inorg. Chem.* **2007**, *46*, 4028-4035, DOI: 10.1021/ic062192q.

[22] Ghambarian, M.; Azizi, Z.; Ghashghaee, M., Cluster modeling and coordination structures of Cu^+ ions in Al-incorporated Cu-MEL catalysts -a density functional theory study. *J. Mex. Chem. Soc.* **2017**, *61*, 1-13, DOI: 10.29356/jmcs.v61i1.122.

[23] Ghambarian, M.; Ghashghaee, M.; Azizi, Z., Coordination and siting of Cu^+ ion adsorbed into silicalite-2 porous structure: A density functional theory study. *Phys. Chem. Res.* **2017**, *5*, 135-152, DOI: 10.22036/pcr.2017.39255.

[24] Ghashghaee, M.; Ghambarian, M.; Azizi, Z., Characterization of extraframework Zn^{2+} cationic sites in silicalite-2: a computational study. *Struct. Chem.* **2016**, *27*, 467-475, DOI: 10.1007/s11224-015-0575-y.

[25] Valiev, M.; Bylaska, E. J.; Govind, N.; Kowalski, K.; Straatsma, T. P.; Van Dam, H. J. J.; Wang, D.; Nieplocha, J.; Apra, E.; Windus, T. L.; de Jong, W. A., NWChem: A comprehensive and scalable open-source solution for large scale molecular simulations. *Comput. Phys. Commun.* **2010**, *181*, 1477-1489, DOI: 10.1016/j.cpc.2010.04.018.

[26] Lu, T.; Chen, F., Multiwfn: A multifunctional wavefunction analyzer. *J. Comput. Chem.* **2012**, *33*, 580-592, DOI: 10.1002/jcc.22885.

[27] Giannozzi, P.; Baroni, S.; Bonini, N.; Calandra, M.; Car, R.; Cavazzoni, C.; Ceresoli, D.; Chiarotti, G. L.; Cococcioni, M.; Dabo, I.; Dal Corso, A.; de Gironcoli, S.; Fabris, S.; Fratesi, G.; Gebauer, R.; Gerstmann, U.; Gougoussis, C.; Kokalj, A.; Lazzeri, M.; Martin-Samos, L.; Marzari, N.; Mauri, F.; Mazzarello, R.; Paolini, S.; Pasquarello, A.; Paulatto, L.; Sbraccia, C.; Scandolo, S.; Sclauzero, G.; Seitsonen, A. P.; Smogunov, A.; Umari, P.; Wentzcovitch, R. M., QUANTUM ESPRESSO: a modular and open-source software project for quantum simulations of materials. *J. Phys.: Condensed Matter* **2009**, *21*, 395502, DOI: 10.1088/0953-8984/21/39/395502.

[28] Macrae, C. F.; Bruno, I. J.; Chisholm, J. A.; Edgington, P. R.; McCabe, P.; Pidcock, E.; Rodriguez-Monge, L.; Taylor, R.; van de Streek, J.; Wood, P. A., Mercury CSD 2.0 - new features for the visualization and investigation of crystal structures. *J. Appl. Crystallogr.* **2008**, *41*, 466-470, DOI: 10.1107/S0021889807067908.

[29] Macrae, C. F.; Edgington, P. R.; McCabe, P.; Pidcock, E.; Shields, G. P.; Taylor, R.; Towler, M.; van de Streek, J., Mercury: visualization and analysis of crystal structures. *J. Appl. Crystallogr.* **2006**, *39*, 453-457, DOI: 10.1107/S002188980600731X.

[30] Perdew, J. P.; Burke, K.; Ernzerhof, M., Generalized Gradient Approximation Made Simple. *Phys. Rev. Lett.* **1996**, *77*, 3865-3868, DOI: 10.1103/PhysRevLett.77.3865.

[31] Perdew, J. P.; Burke, K.; Ernzerhof, M., Errata: Generalized gradient approximation made simple.

Phys. Rev. Lett. **1997**, *78*, 1396-1396, DOI: 10.1103/PhysRevLett.78.1396.

[32] Hariharan, P. C.; Pople, J. A., Accuracy of AHn equilibrium geometries by single determinant molecular orbital theory. *Mol. Phys.* **1974**, *27*, 209-214, DOI: 10.1080/00268977400100171.

[33] Francl, M. M.; Pietro, W. J.; Hehre, W. J.; Binkley, J. S.; Gordon, M. S.; DeFrees, D. J.; Pople, J. A., Self-consistent molecular orbital methods. XXIII. A polarization-type basis set for second-row elements. *J. Chem. Phys.* **1982**, *77*, 3654-3665, DOI: 10.1063/1.444267.

[34] Heyd, J.; Scuseria, G. E.; Ernzerhof, M., Hybrid functionals based on a screened Coulomb potential. *J. Chem. Phys.* **2003**, *118*, 8207-8215, DOI: 10.1063/1.1564060.

[35] Heyd, J.; Scuseria, G. E., Assessment and validation of a screened Coulomb hybrid density functional. *J. Chem. Phys.* **2004**, *120*, 7274-7280, DOI: 10.1063/1.1668634.

[36] Izmaylov, A. F.; Scuseria, G. E.; Frisch, M. J., Efficient evaluation of short-range Hartree-Fock exchange in large molecules and periodic systems. *J. Chem. Phys.* **2006**, *125*, 104103, DOI: 10.1063/1.2347713.

[37] Raghavachari, K.; Trucks, G. W., Highly correlated systems. Excitation energies of first row transition metals Sc-Cu. *J. Chem. Phys.* **1989**, *91*, 1062-1065, DOI: 10.1063/1.457230.

[38] McLean, A. D.; Chandler, G. S., Contracted gaussian basis sets for molecular calculations. I. Second row atoms, Z = 11-18. *J. Chem. Phys.* **1980**, *72*, 5639-5648, DOI: 10.1063/1.438980.

[39] Bader, R. F. W., A quantum theory of molecular structure and its applications. *Chem. Rev.* **1991**, *91*, 893-928, DOI: 10.1021/cr00005a013.

[40] Bader, R. F. W., The quantum mechanical basis of conceptual chemistry. *Monatsh. Chem.* **2005**, *136*, 819-854, DOI: 10.1007/s00706-005-0307-x.

[41] Bader, R. F. W., Molecular fragments or chemical bonds. *Accounts Chem. Res.* **1975**, *8*, 34-40, DOI: 10.1021/ar50085a005.

[42] Bader, R. F. W., Atoms in Molecules: A Quantum Theory. Oxford University Press, 1994.

[43] Matta, C. F.; Boyd, R. J., The Quantum Theory of Atoms in Molecules: From Solid State to DNA and Drug Design. Wiley-VCH Verlag GmbH & Co. KGaA, 2007.

[44] Fukui, K.; Yonezawa, T.; Shingu, H., A molecular orbital theory of reactivity in aromatic hydrocarbons. *J. Chem. Phys.* **1952**, *20*, 722-725, DOI: 10.1063/1.1700523.

[45] Zhu, H.; Zhou, C.; Wang, X.; Chen, X.; Yang, W.; Wu, Y.; Lin, W., Doping behaviors of adatoms adsorbed on phosphorene. *Phys. Status Solidi B* **2016**, *253*, 1156-1166, DOI: 10.1002/pssb.201552586.

[46] Kulish, V. V.; Malyi, O. I.; Persson, C.; Wu, P., Adsorption of metal adatoms on single-layer phosphorene. *Phys. Chem. Chem. Phys.* **2015**, *17*, 992-1000, DOI: 10.1039/c4cp03890h.

[47] Zhiyuan, Y.; Shuangying, L.; Neng, W.; Shan, L.; Haiyun, S.; Hong, Y., Effect of metal adatoms on hydrogen adsorption properties of phosphorene. *Mater. Res. Express* **2017**, *4*, 045503, DOI: 10.1088/2053-1591/aa6ac0.

[48] Roldán, R.; Castellanos-Gomez, A.; Cappelluti, E.; Guinea, F., Strain engineering in semiconducting two-dimensional crystals. *J. Phys.: Condensed Matter* **2015**, *27*, 313201, DOI: 10.1088/0953-8984/27/31/313201.

[49] Qiao, J.; Kong, X.; Hu, Z. -X.; Yang, F.; Ji, W., High-mobility transport anisotropy and linear dichroism in few-layer black phosphorus. *Nat. Commun.* **2014**, *5*, 4475, DOI: 10.1038/ncomms5475.

[50] Rastogi, P.; Kumar, S.; Bhowmick, S.; Agarwal, A.; Chauhan, Y. S., Effective doping of monolayer phosphorene by surface adsorption of atoms for electronic and spintronic applications. *IETE J. Res.* **2017**, *63*, 205-215, DOI: 10.1080/03772063.2016.1243020.

[51] Cai, Y.; Zhang, G.; Zhang, Y. -W., Layer-dependent band alignment and work function of few-layer phosphorene. *Scientific Reports* **2014**, *4*, 6677, DOI: 10.1038/srep06677.

[52] Lv, H.; Lu, W.; Shao, D.; Sun, Y., Large thermoelectric power factors in black phosphorus and phosphorene, 2014.

[53] Ghashghaee, M.; Ghambarian, M.; Azizi, Z.,

Molecular-level insights into furfural hydrogenation intermediates over single-atomic Cu catalysts on magnesia and silica nanoclusters. *Mol. Simul.* **2019**, *45*, 154-163, DOI: 10.1080/08927022.2018.1547820.

[54] Ghambarian, M.; Ghashghaee, M.; Azizi, Z.; Balar, M., Influence of surface heterogeneities on complexation of ethylene with active sites of NiMCM-41 nanocatalyst: A density functional theory study. *Phys. Chem. Res.* **2019**, *7*, 235-243, DOI: 10.22036/pcr.2019.153980.1555.

[55] Ghambarian, M.; Ghashghaee, M.; Azizi, Z.; Balar, M., Structural diversity of metallacycle intermediates for ethylene dimerization on heterogeneous NiMCM-41 catalyst: a quantum chemical perspective. *Struct. Chem.* **2019**, *30*, 137-150, DOI: 10.1007/s11224-018-1184-3.

[56] Ghashghaee, M.; Ghambarian, M., Ethene Protonation Over Silica-Grafted Metal (Cr, Mo and W) Oxide Catalysts: A Comparative Nanocluster Modeling Study. *Russ. J. Inorg. Chem.* **2018**, *63*, 1570-1577, DOI: 10.1134/S0036023618160015.

[57] Ghashghaee, M.; Ghambarian, M., Methane adsorption and hydrogen atom abstraction at diatomic radical cation metal oxo clusters: first-principles calculations. *Mol. Simul.* **2018**, *44*, 850-863, DOI: 10.1080/08927022.2018.1465568.

[58] Ghashghaee, M.; Ghambarian, M., Initiation of heterogeneous Schrock-type Mo and W oxide metathesis catalysts: A quantum thermochemical study. *Comp. Mater. Sci.* **2018**, *155*, 197-208, DOI: 10.1016/j.commatsci.2018.08.031.